Hindawi
International Journal of Aerospace Engineering
Volume 2024, Article ID 6130930, 11 pages
https://doi.org/10.1155/2024/6130930

Research Article

Surface Performance of Titanium Alloy Brake Shell Polished by Industrial Robot Based on Digital Twin

Haijun Zhang,[1] Shengwei Chen,[1] Hui Wang,[2] and Yan Qin[1]

[1]*School of Aeronautics and Astronautics, Zhengzhou University of Aeronautics, 450000, China*
[2]*Research Institute of Aeroengine, Beihang University, 100000, China*

Correspondence should be addressed to Shengwei Chen; kidscsw@gmail.com

Received 29 August 2023; Revised 13 November 2023; Accepted 1 December 2023; Published 8 January 2024

Academic Editor: Zhiguang Song

The titanium alloy brake shell is an important component used in aviation, but its surface polishing is mostly done manually, making it difficult to ensure surface quality and consistency. As a result, an industrial robot polishing system based on digital twin is proposed, which can realize the interaction between physical and virtual platforms by using digital twin technology, acquire various parameters in real time, and monitor the polishing process. Based on this system, a removal depth model was established, and the polishing parameters to be analyzed were determined by combining the removal depth model. On this basis, the influence law of polishing parameters on surface roughness is analyzed through physical tests, and orthogonal experiments are used to optimize the polishing parameters. The results show that the surface roughness is reduced to 0.171 μm after optimization. Finally, the reliability of the polishing system is verified through the polishing machining test, and the surface quality of titanium alloy brake shell is significantly improved.

1. Introduction

Titanium alloy brake shell is one of the mechanisms of aircraft brake assembly and an important titanium alloy component used in the aviation field. Currently, the polishing process for titanium alloy brake shell is mostly done manually, resulting in deficiencies in surface consistency and quality. However, industrial robots are widely used in the field of industrial processing nowadays. Building an industrial robot polishing system based on digital twin for polishing titanium alloy brake shell can achieve monitoring of the polishing process, explore the impact of flap wheel polishing parameters on surface performance, and optimize the polishing parameters, which helps to improve its surface quality and performance, ensure surface consistency, and promote the development of the aviation industry.

Many scholars have conducted research on robot polishing and surface performance. For example, Huai et al. [1] used orthogonal experiments and range analysis to improve the quality of aerospace engine blades and reduce surface roughness. They differentiated primary and secondary polishing parameters and established a polishing roughness prediction model, whose reliability was also verified. Du et al. [2] studied the influence of different processing methods on the surface integrity of TC21 titanium alloy and detected the processed titanium alloy materials. They found that adding TC21 titanium alloy parts through longitudinal polishing after turning can achieve better surface quality and fatigue resistance. Zhao et al. [3] used similar polishing parameters to polish workpieces with different surface roughness and found that workpieces with different roughness can be polished to similar roughness. Xiao et al. [4] proposed a robot abrasive belt polishing mechanism to address the low efficiency and poor consistency in the manual polishing of integral disk blades. The results indicated that the polishing efficiency increased by 1.5 times when compared with manual polishing, the consistency of the polished blade was better, and the surface roughness could reach Ra 0.24 μm. Pan et al. [5] proposed a static stiffness optimization method for robots to eliminate the impact of vibration on the workpiece surface during robot machining. The reliability of the optimization was verified through

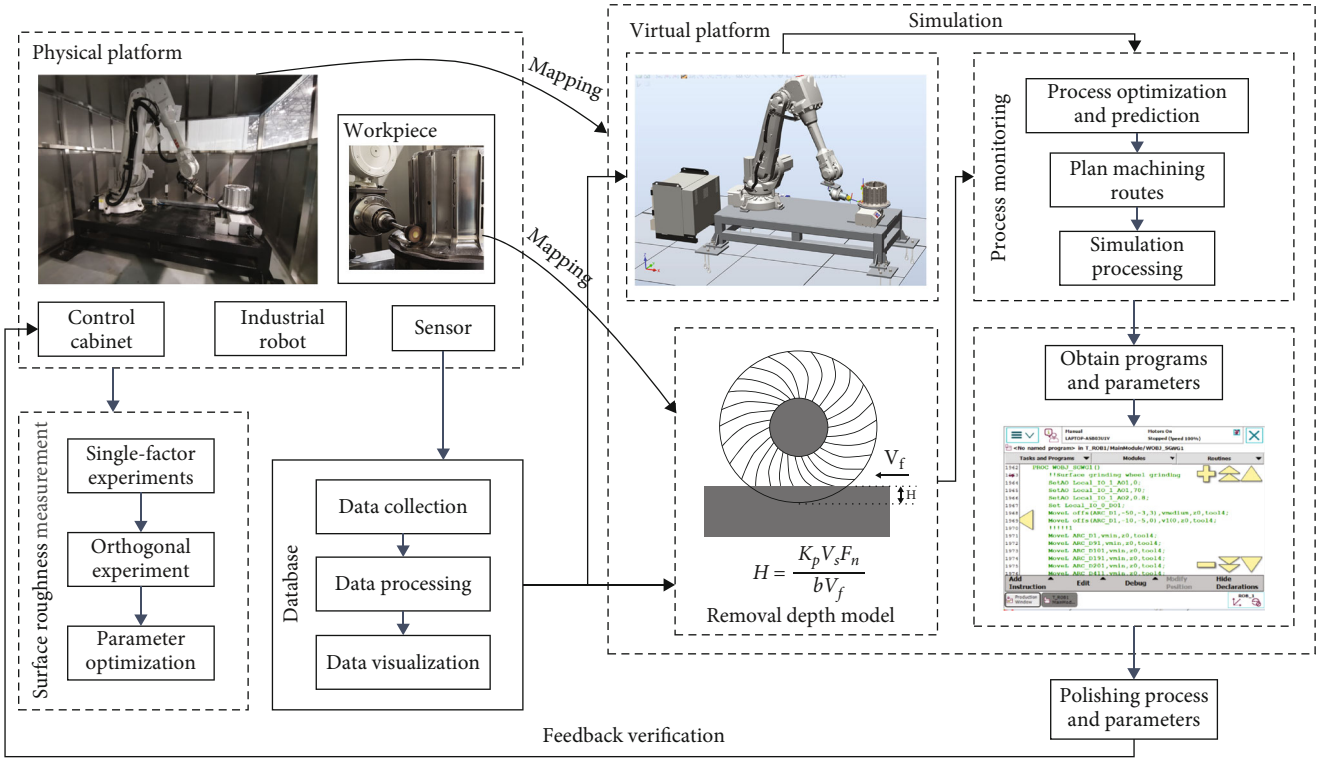

Figure 1: Framework of industrial robot polishing system based on digital twin.

simulation experiments. Results showed that the stiffness of the optimized robot increased by 26.8% and the surface roughness of the workpiece increased by 42.9%. Zhang et al. [6] studied the removal depth model during robot polishing of blades, and they combined the model with a mathematical model of microforce distribution for single and multiple abrasive grains on the blade surface to analyze the micromaterial removal on the blade surface. In the study, a material removal model for grinding wheel polishing of blades was established, and the reliability of the removal depth model was verified through experiments. Mohammad et al. [7] proposed a robot equipped with an end-effector force controller for automatic polishing, which can effectively reduce vibration and achieve force control. Zhu et al. [8] discussed the problems and challenges faced by robots in grinding complex parts in terms of precision control, flexibility control, and cooperative control, and they analyzed the impact on the geometric accuracy, surface integrity, and processing efficiency of the processed workpiece. Pandiyan et al. [9] developed a robot-based abrasive belt grinding device and pointed out the nonlinear relationship between the removed material and the process variables. They determined the removal amount through the ANFIS model. Zhang et al. [10] proposed a roughness measurement method based on GAN and BP neural networks for free-form surfaces with large curvature variations. Experiments have shown that the accuracy of this method can measure free-form surfaces with a minimum roughness of 0.2 μm, with an error of 10% in the results. Shaw and Fang [11] proposed a grinding and polishing system with a robotic gripper handheld grinder and a force control mechanism to address the drawbacks of manual polishing. Experiments have shown that this system can reduce the surface roughness of 340 stainless steel. Ma et al. [12] designed and constructed a robotic belt grinding automation production system for complex surface workpieces to address the problems of the lack of engineering practice in robotic grinding. Dieste et al. [13] investigated the effects of parameters and material removal on precision machining based on the spherical robot automatic grinding and polishing system, in order to improve the surface quality of the workpiece. Zhu et al. [14] established a microscopic scale of cutting force model using a robotic belt grinding mechanism and conducted experiments on force control to investigate the effect of force control on the surface roughness of the workpiece. Zhong et al. [15] discussed the polishing technology for the precision manufacture of aspheric optics based on robots, conducted experiments using this polishing system, and achieved good results to verify the reliability of the polishing technology. This provides an efficient, low-cost, and high-precision manufacturing technology for scholars. Tian et al. [16] established a removal depth model based on a robotic grinding platform, analyzed the influence of grinding parameters on the removal depth, obtained the optimal parameters through orthogonal experiments, and removed the aluminum clad of aircraft skin. An [17] designed a robot end grinding tool and built a robot automatic grinding platform, based on which the removal characteristic analysis and grinding process test were carried out, realizing the robot automatic grinding and polishing of free-form surfaces.

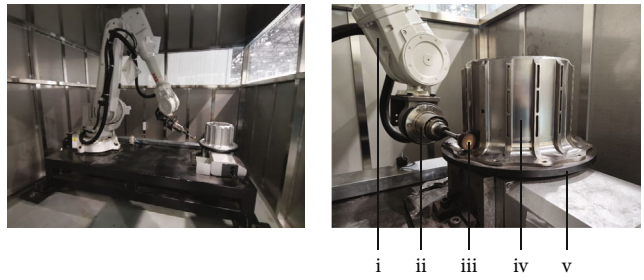

Figure 2: Physical polishing system: (a) the whole platform and (b) details with (i) industrial robot, (ii) floating electric spindle, (iii) flap wheel, (iv) titanium alloy brake shell, and (v) servo turntable.

In the above research, there are the following issues:

(1) The tools used in most robot polishing systems are not universally applicable and cannot be effectively applied to surfaces with significant curvature changes

(2) There is no corresponding monitoring system for the robot polishing process, which prevents real-time understanding of the problems that occur during the polishing process

For the above problems, this paper proposes the following solutions:

(1) Aiming at the structure of the titanium alloy brake shell, this paper proposes the end polishing mechanism of the floating electric spindle clamping flap wheel to avoid the processing interference problem

(2) Build an industrial robot polishing system based on digital twin, which can deeply understand the polishing process by using digital twin technology and realize the functions of virtual and real interaction, real-time monitoring, etc. The system includes three parts: the physical platform, the database, and the virtual platform

In this paper, the polishing process of titanium alloy brake shell is studied on the basis of the above, the removal depth model is established, and the main polishing parameters are determined. Through single-factor experiments to study the main polishing parameters on the material surface properties of the influence of the law, based on orthogonal experiments to determine the optimal polishing parameters, the titanium alloy brake shell was polished and processed and achieved good processing results.

2. Industrial Robot Polishing System Based on Digital Twin

Built on industrial robots, the industrial robot polishing system based on digital twin establishes a mirrored digital twin that can monitor the system status and surface roughness during the polishing process through interaction between physical and virtual platforms. The framework system is shown in Figure 1. The system mainly consists of a physical platform, a database, and a virtual platform. The physical platform includes industrial robot and workpieces. The database mainly collects and processes dynamic and static data during the polishing process. The virtual platform mirrors the physical platform, which can achieve virtual simulations and provide feedback on the simulation results to the physical platform.

Table 1: Correspondence between air pressure and floating force.

Air pressure (Bar)	Floating force (N)
0-0.6	0
1	15
2	52
3	89
4	126

2.1. Construction of Physical Polishing Platform. The physical polishing platform is mainly composed of a six-degree-of-freedom ABB-IRB4600 industrial robot, a floating electric spindle, a control cabinet, a servo turntable, frock, workpieces, and so on, as shown in Figure 2.

The flap wheel is selected as the polishing tool, and the contact between the flap wheel and the workpiece is in the form of flexible contact, which reduces the occurrence of overpolishing, underpolishing, and interference. The floating electric spindle used for polishing is controlled by a frequency converter, with a maximum speed of 24000 r/min. The electronic proportional valve is used to control the air pressure of the airbag and adjust the floating force. By changing the floating force, pressure control during the polishing process can be achieved. The floatable angle is ±5°. The corresponding relationship between air pressure and floating force is shown in Table 1. Moreover, an extension rod is used to prevent interference during the polishing process, as show in Figure 3.

2.2. Construction of Virtual Polishing Platform

2.2.1. 3D Model. The commonly used 3D software in mechanical engineering includes Pro/Engineer, UG, SolidWorks, and

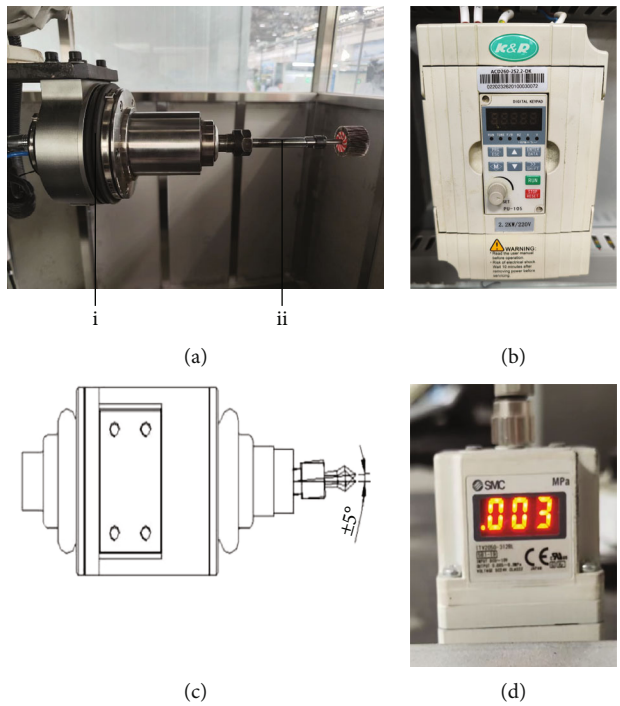

Figure 3: Main functions of floating electric spindle: (a) floating electric spindle with (i) airbag and (ii) extension rod; (b) frequency converter; (c) floating function; (d) electronic proportional valve.

Autodesk Mold flow. This article uses UG to draw a 3D model of the industrial robot polishing system.

2.2.2. Data Collection. Collect both dynamic and static data. For the polished surface, a three-dimensional white light interference surface topography instrument is used to detect its surface profile. The basic parameter data for the polishing processing is obtained from the industrial robot system, including the industrial robot model and industrial robot parameter settings. The driving data of the industrial robot is obtained through communication with RobotStudio, including the position coordinates of the TCP point and the workpiece, the polishing parameters, and the machining program. Sensor data is obtained through external sensors, including the angle of the servo turntable and polishing pressure. All of the above data is ultimately transmitted to the PC through the PLC control cabinet, as show in Figure 4.

2.2.3. Virtual Polishing Platform. Complete assembly of the required 3D model with the ABB-IRB4600 industrial robot model. And then, various actions of the industrial robot are defined. At the same time, the collected data from the industrial robot is integrated and input into the virtual polishing platform. This allows it to capture the robot's polishing processing actions and monitor and simulate the actual polishing process system status and workpiece surface roughness. The virtual polishing platform is illustrated in Figure 5.

2.3. System Operation Mode

(1) Set the polishing parameters and carry out the processing on the physical polishing platform

(2) Collect static and dynamic data during the polishing process from the sensors in the system, and input the data into the virtual platform through the PLC control cabinet

(3) Receive the data on the virtual platform from RobotStudio and perform polishing simulations based on the established base model to achieve realistic mapping and finally optimize polishing parameters through simulations

(4) Connect the virtual platform to the controller through a service port by utilizing the online features of RobotStudio. This enables feedback of various kinds of information and allows the optimized results to be synchronously applied to the physical platform. And the experiments are conducted to verify the polishing parameters

The system operates as shown in Figure 6.

3. The Regularity Analysis of Polishing Removal Depth

3.1. Preston's Empirical Equation. Polishing by flap wheel is a process of material removal. The relationship between the amount of material removal and various process parameters during the machining process can be referred to Preston's equation. The equation is as follows [18]:

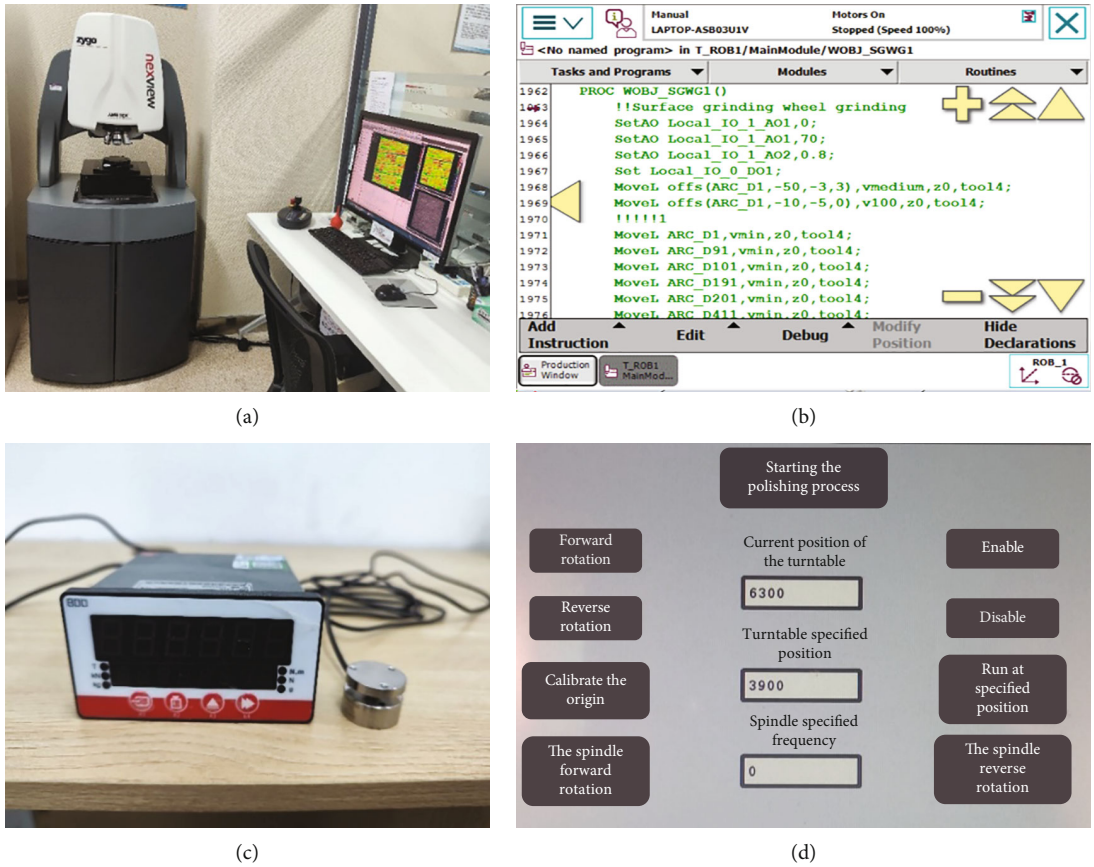

(a) (b)

(c) (d)

Figure 4: Data collection: (a) three-dimensional white light interference surface topography instrument; (b) polishing parameters; (c) pressure sensor; (d) the angle of servo turntable.

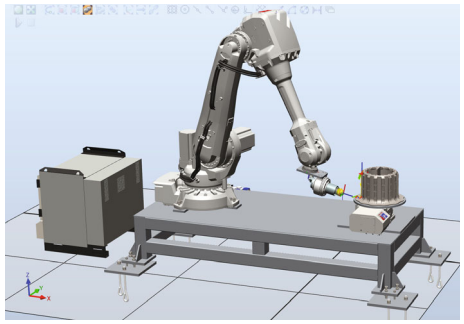

Figure 5: Virtual polishing platform.

$$\frac{dH}{dT} = K_p P V_r \tag{1}$$

In the equation, dH/dT represents the removal depth per unit time, P is the contact pressure, V_r is the relative velocity between the workpiece and the grinding head, and K_p is the wear coefficient. In actual machining, it is a polishing path with a length of dL. The differential form is as follows:

$$\frac{dH}{dL} * \frac{dL}{dT} = K_p P V_r. \tag{2}$$

The expression for the feed rate is as follows:

$$V_f = \frac{dL}{dT}. \tag{3}$$

After substitution and simplification, the expression for the removal depth obtained is as follows:

$$dH = \frac{K_p P V_r}{V_f} * dL. \tag{4}$$

3.2. Removal Depth Model. In actual polishing, the curvature of the workpiece is much greater than that of the flap wheel, which is approximately a plane contact. The contact area is rectangular, and a coordinate system is established with the center of the rectangle as the origin, as shown in Figure 7.

In the contact area between the flap wheel and the workpiece as shown in Figure 7(b), where a represents the polishing length and b represents the wheel width, the expression for the contact area is

$$S(x, y) = \begin{cases} -\frac{a}{2} \le x \le \frac{a}{2}, \\ -\frac{b}{2} \le y \le \frac{b}{2}. \end{cases} \tag{5}$$

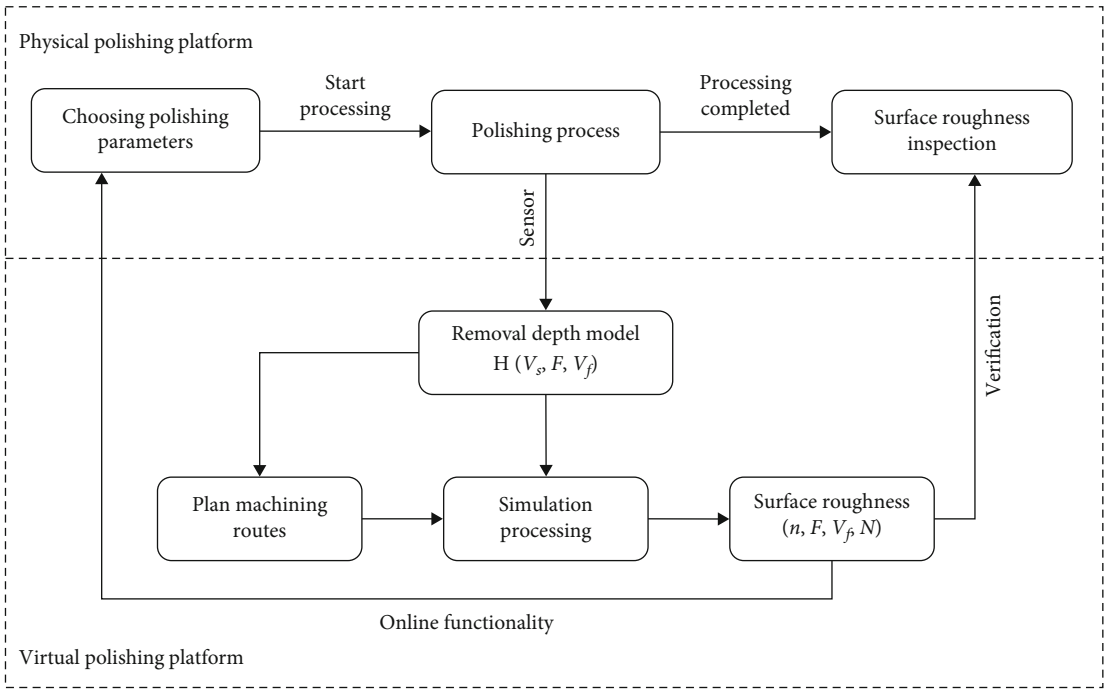

Figure 6: Digital twin-based operation mode.

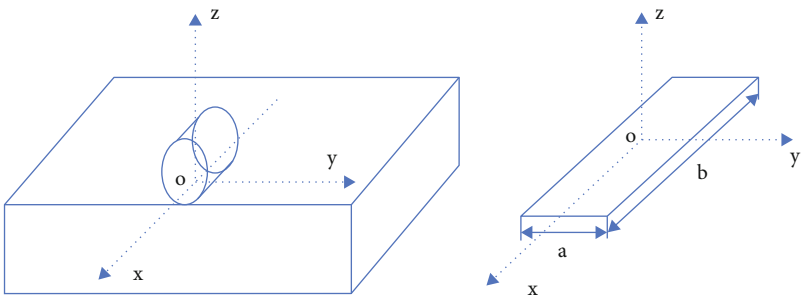

Figure 7: Analysis of plane contact: (a) schematic diagram of plane contact and (b) analysis of the contact area.

The area of the contact region is given by

$$S = a * b. \tag{6}$$

The average pressure in the contact area is denoted as P, and the contact pressure is F_n; then,

$$P = \frac{F_n}{S} = \frac{F_n}{ab}. \tag{7}$$

Substitute it into expression (4) for the removal depth and integrate over the moving distance L:

$$H = \int_{a/2}^{-a/2} \frac{K_p V_r}{V_f} * \frac{F_n}{ab} dL. \tag{8}$$

Table 2: Polishing parameters.

Polishing parameters	Reference value
Spindle speed (r/min)	3500, 4000, 4500, 5000
Pressure (N)	5, 10, 15, 20
Feed rate (mm/s)	5, 10, 15, 20
The mesh of the flap wheel	80, 120, 240, 320

Simplify the above equation:

$$H = \frac{K_p V_r F_n}{b V_f}. \tag{9}$$

Since the actual polishing centerline speed is much greater than the feed velocity V_f, the influence of the feed

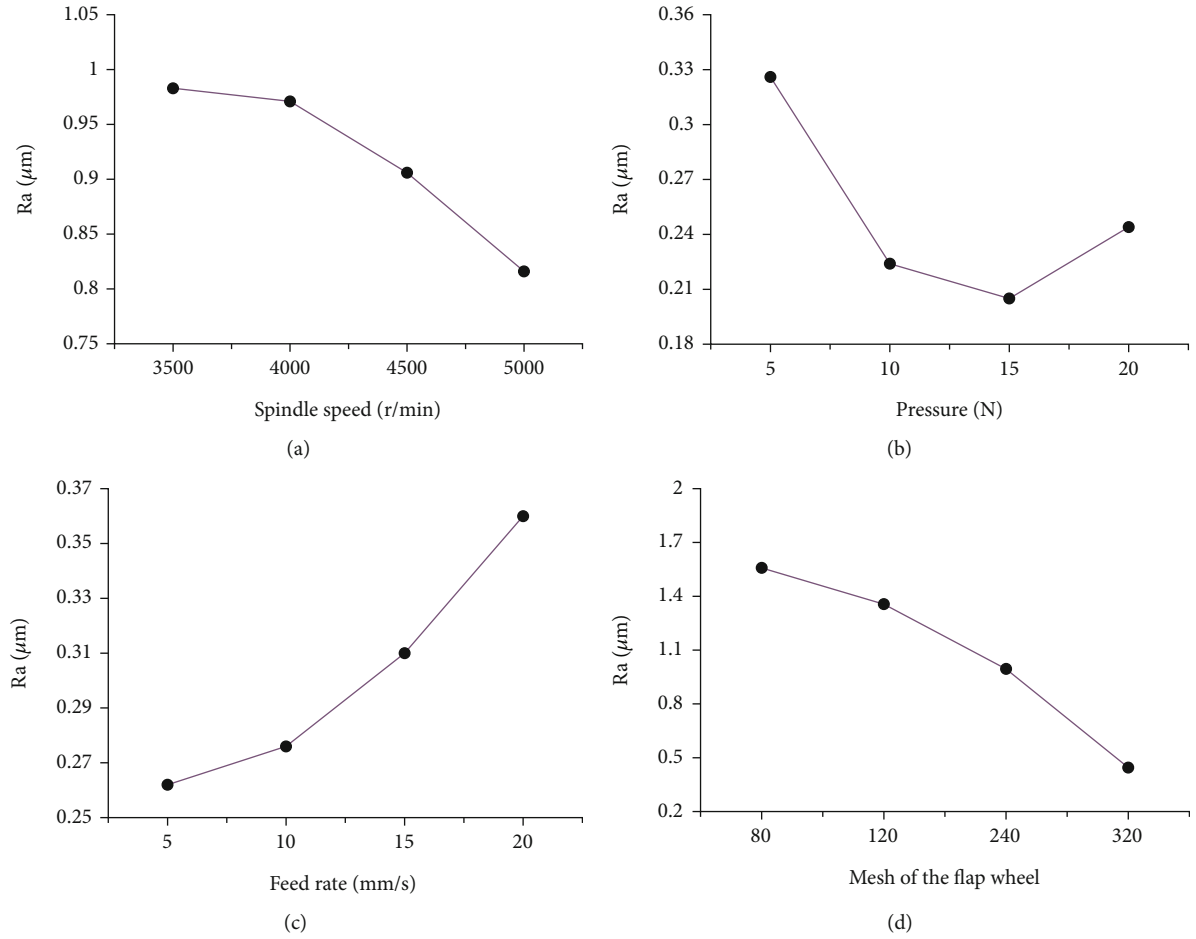

Figure 8: The influence of polishing parameters on surface roughness: (a) the influence of spindle speed on surface roughness; (b) the influence of pressure on surface roughness; (c) the influence of feed rate on surface roughness; (d) the influence of the mesh of the flap wheel on surface roughness.

velocity can be neglected. V_s denotes the linear velocity of the flap wheel, and V_r represents the relative velocity; then,

$$H = \frac{K_p V_s F_n}{b V_f}. \tag{10}$$

The equation shows that the material removal depth H is directly proportional to the contact pressure F_n and the linear velocity of the flap wheel V_s, while it is inversely proportional to the width of the flap wheel b and the feed velocity V_f. Therefore, it is important to choose a suitable combination of polishing parameters.

4. The Surface Performance of Polishing

4.1. The Influence of Polishing Parameters on Surface Roughness. Polishing experiments are conducted on the ground of the developed industrial robot polishing system based on digital twin. To avoid interference with the qualified surface of the titanium alloy brake shell during the process, a flap wheel with a width of 25 mm and a diameter of 40 mm is uniformly used in the experiments. The mesh of the flap wheel will impact the workpiece's surface quality, so it is necessary to consider its influence on the surface performance. A single-factor experiment is carried out by determining the polishing parameters, as shown in Table 2, through a large number of prepolishing tests in combination with the removal depth model.

As can be seen from Figure 8(a), the speed of the polishing spindle increased from 3500 r/min to 5000 r/min, and the surface roughness value of the workpiece is getting smaller and smaller with the increase in the spindle speed. This is because as the spindle speed increases, the flap wheel gradually tends towards a rigid body, and the number of times the wheel acts on the surface of the workpiece per unit time increases, which can effectively remove the protrusions on the surface of the workpiece and improve the surface roughness of the workpiece.

As can be seen from Figure 8(b), the polishing pressure is increased from 5 N to 20 N. With the increase in the pressure, the surface roughness value of the workpiece first decreases and then increases. This is due to the fact that as the polishing pressure increases, the interaction between the wheel and the surface of the workpiece changes from friction to polishing, which has a positive effect on the

Table 3: Factor level.

Factor level	Spindle speed (r/min)	Pressure (N)	Feed rate (mm/s)	The mesh of the flap wheel
1	3500	5	5	80
2	4000	10	10	120
3	4500	15	15	240
4	5000	20	20	320

surface finishing of the workpiece and reduces its surface roughness. When the pressure increases to a certain value, the removed debris and abrasive grains cannot be effectively discharged in time, resulting in their adsorption on the surface of the workpiece, increasing the roughness value of the surface of the workpiece.

As shown in Figure 8(c), the feed rate is increased from 5 mm/s to 20 mm/s and the surface roughness value of the workpiece increases gradually with the increase in feed rate. This is because when the feed rate increases, the wheel spends less time acting in the same position, resulting in a less effective removal effect and an increase in surface roughness.

As shown in Figure 8(d), the mesh of the flap wheel increases from 80 to 320 and the surface roughness value of the workpiece decreases gradually with the increase in the mesh of the wheel. As the mesh increases, the distribution of abrasive grains on the surface of the wheel becomes more uniform, and the abrasive gains are also finer. After polishing, the scratches on the workpiece surface are also more even, along with a decrease in the surface roughness of the workpiece.

By comparing the range of surface roughness values combining Figure 8, it can be concluded that the mesh of the flap wheel has the greatest impact on surface roughness, followed by spindle speed and polishing pressure, while the feed rate has the least impact.

4.2. Optimization of Polishing Parameters. According to the single-factor experiment, the variation range of four main factors A-D is determined: polishing disk speed $n = 3500 - 5000$ r/min, polishing pressure $F = 5 - 15$ N, feed rate $V_f = 5 - 20$ mm/s, and the mesh of the flap wheel 80-320. Then, design $L_{16}(4^4)$ orthogonal experiment and conduct the experiment. The factor level and orthogonal experiment are shown in Tables 3 and 4.

By using the intuitive analysis method in the orthogonal experiment, the relationship between the mean surface roughness and factors is shown in Figure 9. From the figure, it can be seen that the optimal polishing process parameters are A4B3C1D4, which means that the surface roughness value is the lowest when the spindle speed is 5000 r/min, the grinding and polishing pressure is 15 N, the feed speed is 5 mm/s, and the mesh of the wheel is 320.

As shown in Table 4, it can be concluded through the range analysis that the factors in the experiment have the following effects on the surface roughness value in descending order: mesh of the wheel > pressure > spindle speed > feed rate. This is consistent with the conclusions obtained from the single-factor experiment and verifies the correctness of the experimental results.

Table 4: Polishing orthogonal experiment and surface roughness results.

Experiment number	A	B	C	D	Ra (μm)
1	1	1	1	1	1.537
2	1	2	2	4	0.471
3	1	3	3	2	0.971
4	1	4	4	3	0.380
5	2	1	2	3	0.530
6	2	2	1	2	0.850
7	2	3	4	4	0.412
8	2	4	3	1	1.452
9	3	1	3	4	0.402
10	3	2	4	1	1.338
11	3	3	1	3	0.335
12	3	4	2	2	1.157
13	4	1	4	2	1.080
14	4	2	3	3	0.367
15	4	3	2	1	0.906
16	4	4	1	4	0.253
K1	0.840	0.887	0.744	1.308	—
K2	0.811	0.757	0.766	1.015	—
K3	0.808	0.656	0.798	0.403	—
K4	0.652	0.811	0.803	0.385	—
Range	0.188	0.231	0.059	0.923	—

5. Polishing Experiment

Synchronize the optimized polishing parameters into the industrial robot polishing processing program and conduct experiments on the parameters before and after optimization. The results are shown in Figure 10. From the two-dimensional micromorphology and the waveform of the workpiece cross-section in the figure, it can be observed that before optimizing the polishing parameters, the protrusions on the workpiece surface are extremely obvious with unclear polishing marks that are not clear. The roughness value is 1.378 μm. After optimizing the polishing parameters, the surface of the workpiece becomes more regular and smoother so as to see a clear regular polishing processing path. And the surface finish of the workpiece is effectively improved with a reduced roughness value of 0.171 μm.

The optimized polishing parameters are used to polish the titanium alloy brake shell, achieving good polishing results, as shown in Figure 11. It can be seen from the figure that when the titanium alloy brake shell is not polished, there are obvious milling cutter marks. The use of unoptimized parameters for the polishing process removes the original milling cutter marks, but the effect of polishing is worse with noticeable scratch damage. After parameter optimization, the polishing effect is significantly improved, and the processed surface is smoother with a better polishing effect.

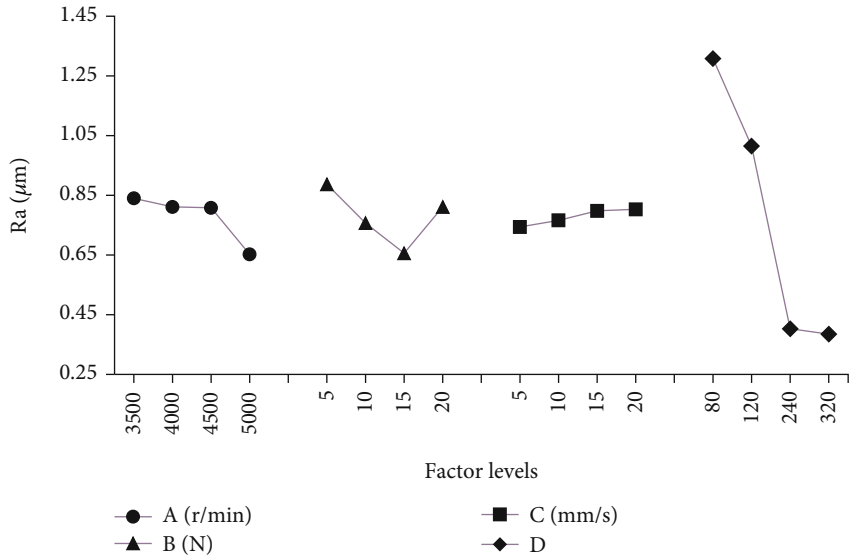

Figure 9: Relationship between surface roughness and factors.

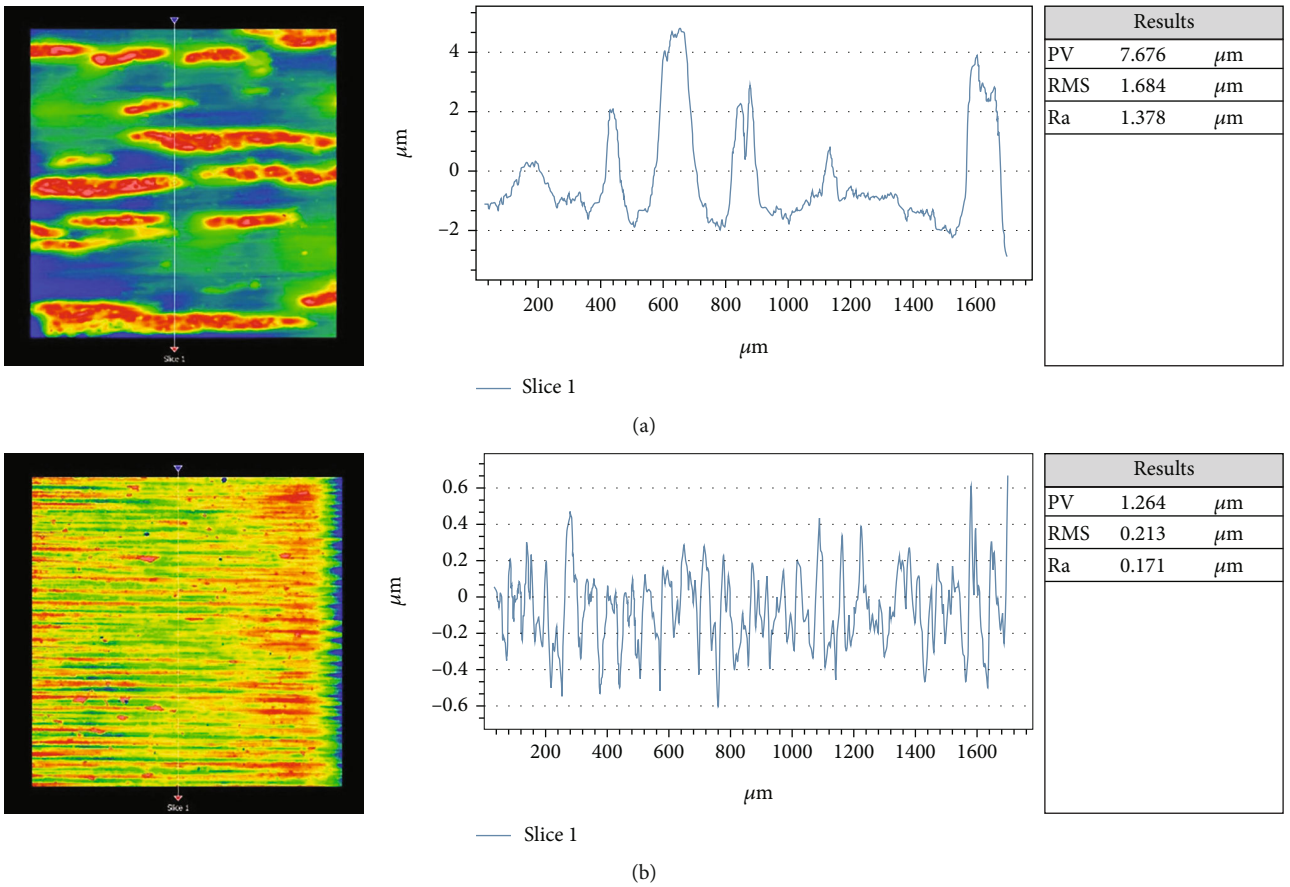

Figure 10: Comparison of polishing results before and after the optimization of the parameters. The figure displays the microscopic two-dimensional morphology and cross-sectional waveform: (a) before the optimization and (b) after the optimization.

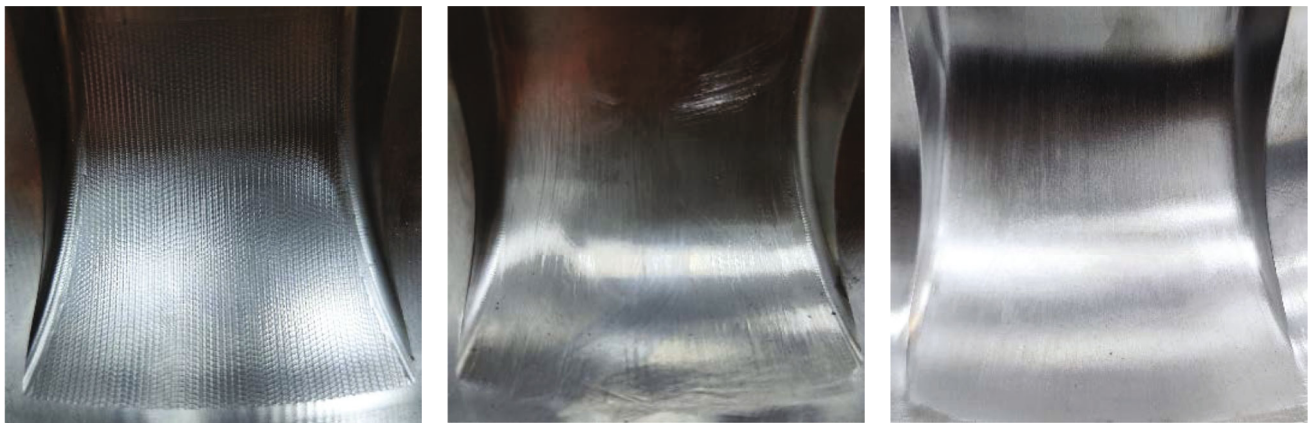

(a) (b) (c)

Figure 11: Comparison of polishing effects: (a) before polishing; (b) nonoptimized; (c) optimized.

6. Conclusion

This paper proposes an industrial robot polishing system based on digital twin and conducts polishing experiments based on this system. The following three conclusions can be drawn.

(1) The industrial robot polishing system based on digital twin is stable and reliable, capable of both physical and simulation processing. It enables mapping and monitoring of the physical platform, allowing for optimization of the polishing process in conjunction with the physical polishing platform

(2) The polishing system used in this study exhibits good controllability and can achieve high surface quality. It contributes to a smaller height difference of the titanium alloy workpieces with a lower surface roughness value. This system effectively addresses the issues associated with manual polishing

(3) In the polishing process of the titanium alloy brake shell, it is of great significance to choose appropriate polishing parameters for improving surface quality. The influence of polishing parameters on surface roughness values is in the following order: mesh > pressure > spindle speed > feed speed. After the optimization of parameters, the surface roughness value of the workpieces is obviously reduced, and the surface quality is greatly improved

Data Availability

The numerical data used to support the findings of this study are available from the corresponding author upon request.

Conflicts of Interest

The authors declare that there is no conflict of interest regarding the publication of this paper.

Acknowledgments

Thanks are due to Dr. Wu Dongbo and Dr. Liang Jiawei from the research group of Tsinghua University for their support in making solutions together. This work is supported in part by the National Natural Science Foundation of China (51705472); Humanities and Social Sciences Foundation of the Ministry of Education of China (22YJAZH144); Supported Project for Science and Technology Research in Henan Province, China (232102320063); and Graduate Educational Innovation Foundation of Zhengzhou University of Aeronautics (2023CX62).

References

[1] W. Huai, Y. Shi, H. Tang, and X. Lin, "Sensitivity of surface roughness to flexible polishing parameters of abrasive cloth wheel and their optimal intervals," *Journal of Mechanical Science & Technology*, vol. 31, no. 2, pp. 865–873, 2017.

[2] D. X. Du, D. X. Liu, Y. F. Sun, J. G. Tang, and X. H. Zhang, "The effects of machined workpiece surface integrity on the fatigue life of TC21 titanium alloy," *Advanced Materials Research*, vol. 503-504, pp. 382–389, 2012.

[3] W. Zhao, I. Mohsin, L. Huang, and K. He, "Surface topography of the metal surface in robot polishing under control force," *Journal of Physics: Conference Series*, vol. 1905, no. 1, 2021.

[4] G. Xiao, K. Song, S. Chen, R. Wen, and X. Zou, "Process analysis and experimental research of robot abrasive belt grinding for blisk," in *2021 6th IEEE International Conference on Advanced Robotics and Mechatronics (ICARM)*, pp. 925–930, Chongqing, China, July 2021.

[5] R. Pan, X. Zhu, Z. Wang et al., "Optimization of static performance for robot polishing system based on work stiffness evaluation," *Engineering Manufacture*, vol. 237, no. 4, pp. 519–531, 2023.

[6] J. Zhang, J. Liu, S. Yang, C. Ju, J. Li, and Z. Qiao, "A model for material removal of robot-assisted blade polishing using abrasive cloth wheel," *The International Journal of Advanced Manufacturing Technology*, vol. 123, no. 7-8, pp. 2819–2831, 2022.

[7] A. E. K. Mohammad, J. Hong, and D. Wang, "Design of a force-controlled end-effector with low-inertia effect for robotic

polishing using macro-mini robot approach," *Robotics and Computer-Integrated Manufacturing*, vol. 49, pp. 54–65, 2018.

[8] D. Zhu, X. Feng, X. Xu et al., "Robotic grinding of complex components: a step towards efficient and intelligent machining - challenges, solutions, and applications," *Robotics and Computer-Integrated Manufacturing*, vol. 65, article 101908, 2020.

[9] V. Pandiyan, W. Caesarendra, T. Tjahjowidodo, and G. Praveen, "Predictive modelling and analysis of process parameters on material removal characteristics in abrasive belt grinding process," *Applied Sciences*, vol. 7, no. 4, p. 363, 2017.

[10] G. Zhang, C. Liu, K. Min, H. Liu, and F. Ni, "A GAN-BPNN-based surface roughness measurement method for robotic grinding," *Machines*, vol. 10, no. 11, p. 1026, 2022.

[11] J. Shaw and Y.-J. Fang, "Development of grinding and polishing technology for stainless steel with a robot manipulator," *Journal of Automation, Mobile Robotics and Intelligent Systems*, vol. 15, no. 4, pp. 37–43, 2022.

[12] K. Ma, X. Wang, and D. Shen, "Design and experiment of robotic belt grinding system with constant grinding force," in *2018 25th International Conference on Mechatronics and Machine Vision in Practice (M2VIP)*, Stuttgart, Germany, November 2018.

[13] J. A. Dieste, A. Fernández, D. Roba, B. Gonzalvo, and P. Lucas, "Automatic grinding and polishing using spherical robot," *Procedia Engineering*, vol. 63, pp. 938–946, 2013.

[14] D. Zhu, X. Xu, Z. Yang, K. Zhuang, S. Yan, and H. Ding, "Analysis and assessment of robotic belt grinding mechanisms by force modeling and force control experiments," *Tribology International*, vol. 120, pp. 93–98, 2018.

[15] B. Zhong, W. Deng, X. Chen, and N. Zheng, "Precision manufacture of aspheric optics by robot-based bonnet polishing," in *Second Target Recognition and Artificial Intelligence Summit Forum*, Changchun, China, 2020.

[16] F. Tian, C. Che, X. Li, and L. Li, "Experiment on micro-removal for aluminum clad of aircraft skin by robotic grinding," *Aeronautical Manufacturing Technology*, vol. 65, no. 13, pp. 56–62, 2022.

[17] H. An, *Complex Curved Surface Robot Automated Polishing Process, [M.S. thesis]*Shenyang Ligong Universityhttps://kns.cnki.net/kcms2/article/abstract?v=2KdPcD7ewrT6uyQna4AZEeZdLU0fenaq4knftbrQD5aXEZFjmzpwsrrksQt7fEHswBaF-ZJHCe2BkyFiFj6mauNzmzIHQVAz70JB0lbwi8jCtaT7COPDNKPQ-br-TXbHvrk2SFt3J02yRJLpeOYjzQ==&uniplatform=NZKPT&language=CHS.

[18] C. Wu, H. Ding, and Y. Chen, "Research on modeling method of material removal depth for CNC mechanical polishing of aluminum alloy wheels," *China Mechanical Engineering*, vol. 21, no. 20, pp. 2558–2562, 2016.